Measuring two-millimeter radiation with a prototype multiplexed TES receiver for ACT

Michael D. Niemack for the ACT Collaboration*

Princeton University Physics Department,
Jadwin Hall, Washington Road, Princeton, NJ 08540, USA

ABSTRACT

The Millimeter Bolometer Array Camera (MBAC) is sheduled for installation on the 6-meter Atacama Cosmology Telescope (ACT) in 2007. MBAC will eventually contain three diffraction-limited, 1024-pixel, focal plane arrays of Transition Edge Sensor (TES) bolometers developed at NASA Goddard Space Flight Center. We present instrument designs and results from optical and electrical measurements made with the MBAC prototype instrument, the Column Camera (CCam). Initial studies with CCam include measurements of the properties of TES detectors, the time-domain SQUID multiplexing readout system developed at NIST Boulder, the Cryoperm magnetic shielding, and preliminary optical measurements with the detectors. We also discuss the status of first light measurements with CCam mounted on a 1.5-meter telescope.

Keywords: detector, TES, bolometer, array, CMB, instrument design, SQUID multiplexing, magnetic shielding

1. INTRODUCTION

The Atacama Cosmology Telescope (ACT) will study the Cosmic Microwave Background (CMB), the oldest light in the universe, on $1.4'$ to one degree scales.[1,2] The CMB is the remnant radiation resulting from the decoupling of photons and baryons 380,000 years after the birth of the universe.[3] The CMB has a 2.7 K black body spectrum and is uniform in temperature at large scales to ten parts per million. Building on a series of ground- and balloon-based measurements,[4] the Wilkinson Microwave Anisotropy Probe (WMAP)[3] has measured the CMB power spectrum, how the temperature fluctuations in the CMB vary with angular scale, at resolutions as fine as 0.3°. The data from these experiments have allowed us to measure many properties of the Universe with unprecedented accuracy. By measuring finer angular scales, one can probe the quantum mechanical properties of the fields that gave rise to the universe. At still finer scales, secondary mechanisms such as the Sunyaev-Zel'ovich (SZ) effect,[5] the Ostriker-Vishniac effect,[6] and gravitational lensing are predicted to be the dominant sources of anisotropy in the CMB.

Associating the CMB observations with optical and X-ray observations is an integral component of understanding these measurements. To this end, members of our collaboration have dedicated time on optical telescopes, including the South African Large Telescope and Chilean telescopes, and have applied for time on X-ray observatories (Chandra and XMM) to study the ACT field. Through combining these multi-frequency measurements, we aim to constrain the equation of state of the universe, probe light neutrino masses down to $m_\nu \simeq 0.1$ eV, and map the mass distribution in the local universe. Such science will require measurements of the temperature of the CMB in multiple frequency bands near the null in the SZ spectrum ($\sim$ 220 GHz), with an accuracy of a few μK at resolutions down to an arcminute.

Large format arrays of millimeter wavelength detectors are required to make measurements with this sensitivity. The ACT collaboration is developing the technology to field novel, close-packed, kilo-pixel arrays of pop-up device (PUD) TES bolometers, conceived at GSFC.[7] Three of these arrays will be installed in the Millimeter Bolometer Array Camera (MBAC). Each array will operate at a different frequency (145 GHz, 225 GHz, and

* The ACT collaboration includes members at: Cardiff U., Columbia U., CUNY, Haverford College, INAOE, NASA/GSFC, NIST/Boulder, Princeton U., Rutgers U., U. British Columbia, U. Católica de Chile, U. KwaZulu-Natal, U. Massachusetts, U. Pennsylvania, U. Pittsburgh, and U. Toronto.

Send correspondence to mniemack@princeton.edu

Millimeter and Submillimeter Detectors and Instrumentation for Astronomy III,
edited by Jonas Zmuidzinas, Wayne S. Holland, Stafford Withington, William D. Duncan,
Proc. of SPIE Vol. 6275, 62750C, (2006) · 0277-786X/06/$15 · doi: 10.1117/12.673038

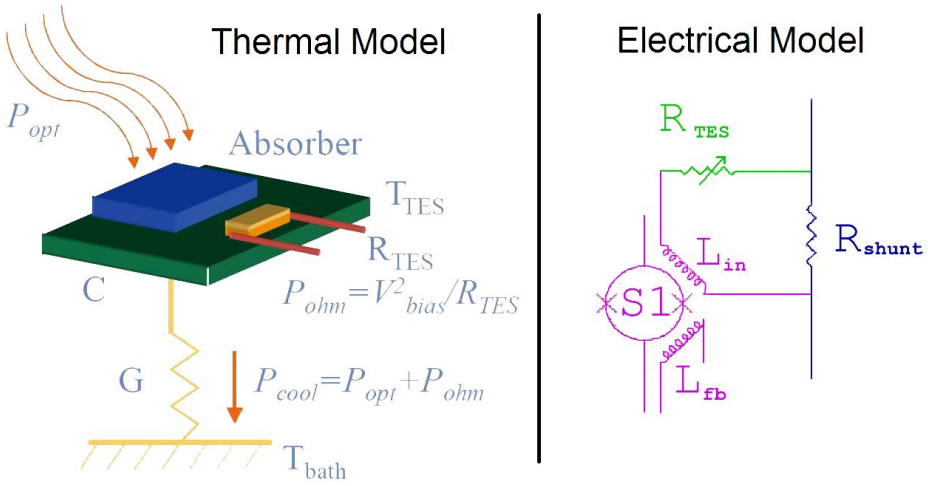

Figure 1. First order models of TES bolometers. Left: The thermal model for a TES bolometer (figure courtesy of D. Benford) is described in section 2.1. Right: The TES electrical model, including the stage 1 (S1) SQUID for measuring current through the TES is described in sections 2.1 and 2.2. Each color in the electrical model represents a different microfabricated chip, as shown in figure 2.

265 GHz) and be fed by three anti-reflection-coated cryogenic silicon lenses.[8] When combined with the 6 m off-axis, aplanatic Gregorian design of the ACT telescope, these lenses generate diffraction-limited images across all three arrays.[9] The ACT telescope is being constructed by AMEC[†] and is scheduled for installation in the Atacama Desert, Chile by the fourth quarter of 2006.

In this paper we describe design considerations for the ACT project and measurements made with the Column Camera (CCam), the MBAC prototype instrument. We report on testing of prototype PUD TES detectors and the readout system used to measure the bolometers as well as the first sky measurements made with PUD TESs.

2. DETECTORS AND READOUT

The three MBAC cameras will each be composed of a 32 × 32 array of TES bolometers[10,11] and will be read out by time-domain SQUID multiplexing electronics.[12,13] The final designs of the MBAC bolometers and the bolometer arrays are nearing completion and will be reported in future publications. A preliminary design is detailed in Marriage, Chervenak, and Doriese.[14] In section 3 we describe results from prototype bolometers fabricated by our collaborators at NASA GSFC's Detector Development Laboratory to aid in the bolometer design optimization and to test prototype technologies for MBAC.

2.1. Detector Overview

During operation, the bolometers are biased at their superconducting transition temperature ($T_c \sim 0.4$ K), where they remain locked through negative electrothermal feedback. A positive CMB temperature fluctuation increases the photon loading, P_{opt}, on the TES, raising its temperature and thereby increasing its resistance. The detectors are approximately voltage biased, with a small parallel shunt resistance (Figure 1), so that the Joule heating $P_{ohm} = V_{bias}^2/R_{TES}$ decreases as the resistance, R_{TES}, rises, which cancels the increase in photon power through a reduction in current.[10,11] The change in current is the signal we measure, as described below.

The bolometers are fabricated as modular columns of 32 TESs, each on a thin silicon absorbing membrane (Figure 2). They are pop-up devices (PUDs), which can be folded and stacked, allowing close packing of multiple columns when building an array.[7] The ability to close-pack these bolometers allowed design of an optical system

[†]AMEC Dynamic Structures, Ltd.,1515 Kingsway Ave., Port Coquitlam, BC V3C 1S2, Canada,
Tel. 604-941-9481 Fax. 604-941-7447

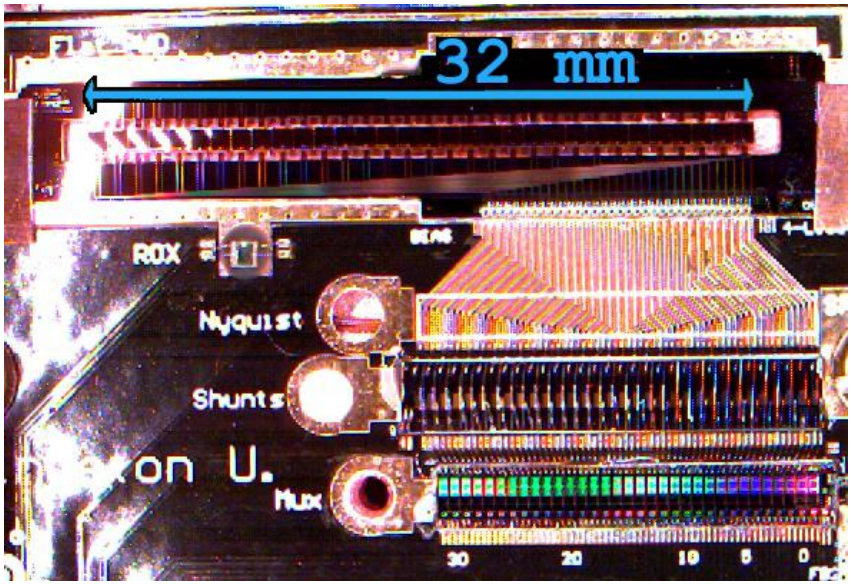

Figure 2. The first TES PUD bolometers ever used to measure mm-wavelength radiation from the sky. One column of 32 detectors (top) and the 0.3 K readout electronics, including the SQUID multiplexing chip (bottom right) and shunt resistor chip (above multiplexing chip), are mounted and wirebonded onto a circuit board. Similar detectors to these are currently being folded onto silicon cards[14] for insertion into an array, however, all bolometers going into arrays will be 1.05 mm on a side, as opposed to the 1.00 mm detectors shown here.

with $1/2F\lambda$ spacing between the detectors, which is optimal for sky sampling in a number of measures.[15] Previous CMB experiments have used feedhorns to couple to detectors, which makes packing the detectors this closely impossible and thus prevents fully sampling the sky with a single array image.

The PUD bolometers have weak thermal links, which also act as supporting legs, connecting them to the surrounding silicon cards. The legs' thermal conductance, $G = dP_{cool}/dT_{TES}$ (Figure 1), determines the maximum power that can be carried away from the absorber, the saturation power of the detectors. If G is too low the detectors will saturate and be useless, and if G is too high thermal noise will dominate the detector signals, decreasing sensitivity to the CMB. By modeling the predicted sky loading at our observing site and the loading from each of the optical components, we have calculated the G's that will be required for each frequency band. In section 3.1 we describe measurements made to determine the leg geometries required to achieve these G values for a given detector T_c.

A related parameter to the thermal conductance is the detector time constant, τ_{det}, which is determined by interactions between the natural thermal time constant, $\tau_{therm} = C/G$ where C is the bolometer heat capacity, and the electrical time constant,[11] $\tau_{el} = L/R_{eff}$ where L is the total inductance in the TES loop including the SQUID input inductance, L_{in}, and R_{eff} is an effective loop resistance. In general, the optimal τ_{det} is constrained from both directions. The upper limit on τ_{det} is imposed by sky sampling. The proposed scan strategy for ACT is to fix the elevation and scan the entire telescope in azimuth up to 5° peak-to-peak and as fast as 0.2 Hz to overcome detector $1/f$ noise. This strategy allows us to avoid scanning through the large atmospheric temperature gradient caused by moves in elevation. In addition, scanning the same region of the sky to the East and West of the South Celestial Pole at elevations higher than the latitude will allow us to crosslink the maps. Crosslinking is one of the critical scan features that contributes to the success of WMAP[3] among other experiments. At 45°elevation, the scan strategy results in a maximum scan rate across the sky of $f_{sky} = 1.5°/\mathrm{s}$. With a resolution of $\sim 52''$ at our highest frequency, we find that to fully sample the sky, $\tau_{det} \leq 400\ \mu\mathrm{s}$; however, preliminary $1/f$ measurements of prototype detectors indicate that we may be able to reduce our scan frequency, which would increase the maximum acceptable τ_{det}. The lower limit on τ_{det} is imposed by the detector sampling frequency as described in section 2.2.

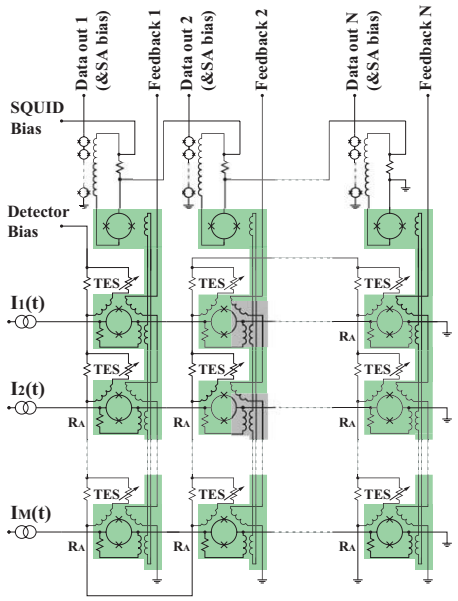

Figure 3. Schematic of a two-dimensional multiplexing array. The row addressing lines, $I_m(t)$, are connected in series resulting in a reduction in the number of wires required to 12 per column for a square array.[13] The components of each multiplexing chip are highlighted, including the S1 SQUIDs and the transformer loop through which they are all coupled to a S2 SQUID. The S2 SQUIDs are the top highlighted device in each column. The series arrays are the small, not highlighted, SQUIDs at the top left of each column. (Figure courtesy of C. D. Reintsema[13])

2.2. Readout Electronics

The required voltage biasing of the TESs means that they must be read out by a current measuring system. Our collaborators in the NIST Quantum Sensors group have developed a time-domain SQUID multiplexing system for reading out the detectors.[12,13] Each TES is connected in series to an inductor, which is magnetically coupled to a DC superconducting quantum interference device (SQUID, Figure 1). When the SQUIDs are current biased, they convert the changing magnetic flux, ϕ, from the inductors into a voltage response,[16] $V(\phi)$. The SQUIDs are inherently nonlinear devices; however, they are kept in the linear regime by warm digital feedback (DFB) electronics, which use a proportional, integral (PI) servo loop to tune the feedback flux response, canceling the input signal to the SQUID from the TES. The recorded signal from the detectors is actually the calculated feedback response applied by the DFB electronics[‡].

If operated independently, each of these SQUIDs would require a minimum of four wires (two biasing/output and two flux feedback),[12] so a 32 × 32 detector array would require 4096 readout wires, not including the TES biasing lines. Multiplexing of the SQUID electronics dramatically reduces the number of connections between room temperature data acquisition electronics and cold detectors. A time-domain multiplexed system like the NIST system, which successively acquires data from each of the 32 rows of TESs in each column, reduces the wire count from 4096 to 384 lines[13,18] (Figure 3). Wire count reduction is important for multiple reasons: 1) space constraints (the entire detection surface in a camera will be $\sim$ 33 mm × 33 mm), 2) limiting thermal conduction into the cryogenic system, and 3) reducing the number of connections. Limiting thermal conduction is particularly important, because increased thermal load increases the cryogenic base temperature, which in turn increases the detector noise and lengthens the observation time required to detect and measure the CMB.

The readout system consists of three stages of SQUIDs[19] (Figure 3). Every TES is connected in series to the

[‡]The tests described in this paper used room temperature DFB electronics developed at NIST/Boulder, however, MBAC will use DFB electronics based on the SCUBA-2[17] system, which will be provided by our collaborators at the University of British Columbia.

input coil, L_{in}, of its own stage 1 (S1) SQUID. Each of these S1 SQUIDs has a corresponding feedback coil, L_{fb} (Figure 1), where feedback flux is applied to cancel the effect of a change in TES current. As described earlier, this S1 feedback flux is the signal that we record. One multiplexing chip contains a column of 33 S1 SQUIDs and a common transformer coil that couples them into a single stage 2 (S2) SQUID. Inputs for 32 of the S1 SQUIDs are connected to TESs, while the 33^{rd}, or "dark", SQUID has an open input. By sampling this 33^{rd} SQUID in series with the others, then smoothing it and subtracting it from the channels with TESs, we can reduce the low frequency noise level,[19] so that it scales as $1/f$ instead of $1/f^2$. These multiplexing chips are mounted onto the same silicon cards as the detectors[14] (Figure 2) and are operated at 0.3 K. The S2 SQUIDs are approximately voltage biased by connecting each in parallel with a 0.1 Ω shunt resistor (Figure 3), which allows us to measure the change in current through each S2 SQUID by an amplifying series array (SA) of 100 SQUIDs operated at 4 K. The SA is current-biased and changes in voltage across it are measured through a standard preamplifier circuit.

The S2 SQUID dynamic resistance is $R_{S2} \approx$ 2-4 Ω,[20] which makes it critical that the wiring between the 0.3 K S2 SQUID and the 4 K SA be low-resistance to maximize gain and low-inductance to minimize the electrical time constant, $\tau_{L/R}$. To accomplish this, in CCam we use 38 AWG superconducting Niobium-Titanium (NbTi) twisted pairs with $\sim$ 5 twists/cm. We have measured the inductance of the NbTi pairs to be $3.5 \pm .7$ nH/cm. Thermal isolation constraints drive us to use $\geq$ 38 cm cables, and adding in the inductances of the SA input and the circuit boards gives us the total measured inductance of the loop $L_{S2-tot} = 0.29 \pm .05$ μH. When R_{S2} is at the minimum of its range, we find that $\tau_{L/R} \approx 0.15$ μs. Ignoring capacitive effects, the circuit will reach 99.9% of its DC value in $7\tau_{L/R} \approx 1.0$ μs. We can use this to estimate the maximum row switching rate, or line rate $f_{line} \leq (7\tau_{L/R})^{-1} \approx 1$ MHz, because this is the minimum time we wait for the S2 loop to settle between turning on the bias to a row of S1 SQUIDs and measuring the output of that row on the series arrays.

As noted in section 2.1, the upper limit on f_{line} imposes a lower limit on τ_{det}. In CCam, we have recently multiplexed a column of bolometers as fast as $f_{line} = 0.5$ MHz. Multiplexing 33 rows at this rate with minimal Nyquist sampling of the detectors gives us a lower limit of $\tau_{det} \geq 33/(\pi f_{line}) = 22$ μs, which is comfortably below the sky sampling limit. Despite the two constraints on τ_{det}, there is a large range of acceptable detector time constants, 22 μs $\leq \tau_{det} \leq$ 400 μs, and one can add inductance to the TES loop to optimize the detector response within this range.[11]

Before using the multiplexing chips to measure detectors, all of the chips for MBAC will be tested individually in a liquid Helium dip probe. This is critical, because all S1 SQUIDs for a given row will be biased in series, so they must have similar critical currents. Also, if there is a discontinuity in any SQUID, it would disable the readout for an entire row of detectors. Because of the sensitivity of an array to discontinuities and point failures, there are multiple additional stages of testing planned, including: testing of each individual column of detectors after assembly with shunt and multiplexing chips as well as testing of 8 × 32 sub-arrays prior to assembly into each 32 × 32 array for MBAC.

2.3. Magnetic Shielding

One difficulty with this readout system is the inherent sensitivity of SQUIDs to magnetic fields. All SQUIDs are encased in magnetic shielding to prevent them from coupling to the gradient in earth's magnetic field as we scan the telescope as well as pickup from any other field sources, like power supplies or motors. The S2 SQUID is effectively the most sensitive component in the readout system to changing magnetic fields, in part because of the large transformer loop between the S1 and S2 SQUIDs. The critical temperatures of the TESs are also affected by magnetic fields; however, we measured this effect to be orders of magnitude smaller than the S2 SQUID response. Measurements of the S2 SQUID sensitivity to applied fields allow us to estimate that we need to attenuate the earth's field by $\sim 10^6$ to reduce scan synchronous field pickup to the projected noise level. Multiple layers of high permeability materials are required to achieve attenuations of this order near our scan frequency.

The dark SQUIDs measure residual magnetic fields without the added confusion of the TES signals. These data can be smoothed and used to subtract the fields from other channels.[19] In general, the responsivity of the bolometers is characterized by variable TES and bolometer parameters and other constant factors, like mutual inductances and resistances.[11] Since a servo loop is used to make null measurements of the TES currents, as long

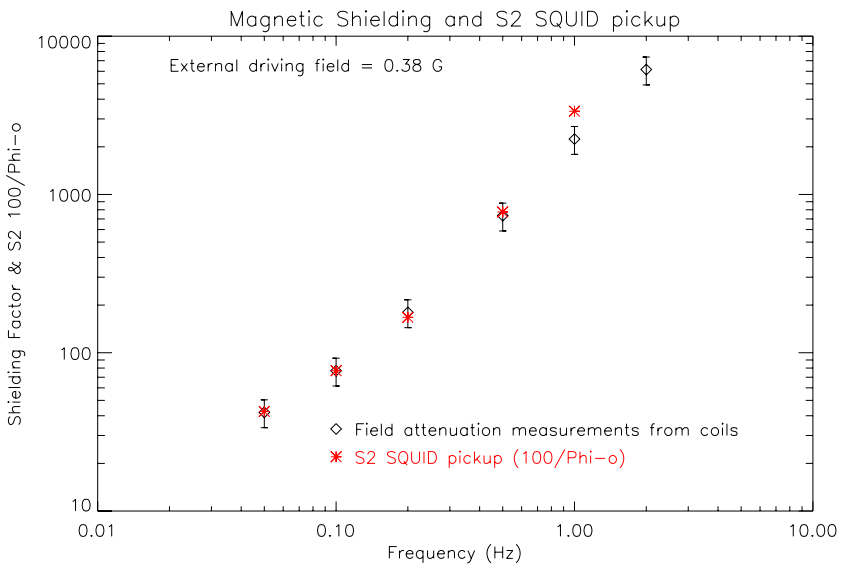

Figure 4. Magnetic field attenuation or shielding factor measurements as a function of frequency for a single layer cylinder of Cryoperm along the z-axis of the cylinder. The attenuation amplitudes are highly geometry dependent, but we have observed a similar increase in attenuation with frequency in other Cryoperm systems. As indicated by the figure, the attenuation measurements, which were made with a cold test coil, are a good proxy for magnetic coupling into the S2 SQUID at these frequencies. Error bars on the S2 measurements are smaller than the plotted points.

as the SQUIDs and PI parameters are tuned properly and the magnetic field does not drive the SQUIDs into a regime in which the PI servo fails, none of the SQUID parameters enter the system gain equation. On the other hand, the slope of the SQUID's $V(\phi)$ curve at the lock-point does affect the transfer function between the error signal (SA output) and the PI-calculated-flux-bias applied to the S1 SQUID. Thus, a magnetic-field-induced change in slope along a SQUID's $V(\phi)$ curve is equivalent to changing the PI servo parameters by the same ratio. This can affect the high-frequency response of the PI loop, but since we sample and servo the detectors at ≥ 10 kHz, and the sky signals we are interested in are measured at ≤ 400 Hz, this should not impact the data so long as the SQUID pickup is much smaller than a magnetic flux quantum.

We studied the shielding properties of Cryoperm, a high-permeability material annealed for use at low temperatures, marketed by Amuneal[§]. Shielding factor, or field attenuation, measurements were made by driving an AC magnetic field from outside the CCam cryostat, and measuring the inductive pickup on a cold test coil located inside a 4 K Cryoperm shield. We simultaneously measured the effect of the field on the S2 SQUID and found that in this frequency range the inductive pickup on the test coil was a good proxy for magnetic coupling into the S2 SQUID (Figure 4). The shielding factor measurements were calibrated by measuring the inductive pickup with the coils in the same configuration without the Cryoperm. We found that the on-axis attenuation of a single cylindrical layer of Cryoperm increases substantially with frequency in the 0.1-2 Hz range (Figure 4). A frequency dependence of the observed magnitude was unexpected. We believe the increase in attenuation with frequency in this range is amplified by a field canceling resonance that occurs in finite cylinders with open ends[21] at $f_{res} = 10^7\rho/(4\mu d^2) \approx 6$ Hz, where $\rho = 0.35\ \Omega\text{mm}^2/\text{m}$ is the specific resistance, $\mu \approx 70,000$ is the permeability at 4 mA/cm quoted by Amuneal, and $d = 1.5$ mm is the Cryoperm thickness. We are continuing to study this phenomena. Thus, in addition to reducing the impact of $1/f$ noise on the data, increasing the scanning frequency also improves the effective magnetic shielding.

[§]Amuneal Manufacturing Corp., 4737 Darrah Street Philadelphia, PA 19124, USA Phone: 215.535.3000 Fax: 215.743.1715, http://www.amuneal.com

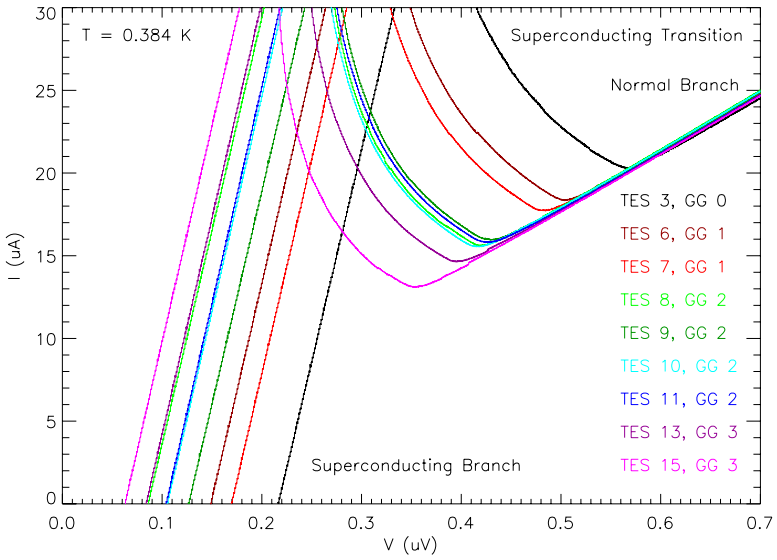

Figure 5. I-V curves acquired at $T_{bath} = 384$ mK for 10 bolometers from a column of TESs with multiple G values. (The data for each bolometer is a different color.) The alignment of the normal branch of the curves indicates that the bolometers on this test device have nearly identical normal resistances, $R_N = 28 \pm 2$ mΩ. We expect TESs in the same G-group, GG, to have similar superconducting transitions as well. This is largely true in the data presented with the exception of GG 3 in which the transition of TES 13 is shifted to higher voltage than expected. The shift could have been caused by a fractured leg, which is difficult to detect prior to folding. The superconducting branches have arbitrary voltage offsets in this plot.

3. PROTOTYPE MEASUREMENTS

We are currently testing the majority of the critical design features planned for MBAC in the Column Camera (CCam). The primary differences between the two designs are that CCam will only test one of the three MBAC bands (145 GHz) and the CCam optics are designed to fully illuminate up to 8×32 detectors instead of three arrays of 32×32 detectors. The CCam optics can couple the detectors to the ACT 6 m telescope or to a smaller telescope as described below.

3.1. Dark Detector Tests

Preliminary detector testing in CCam focused on measuring the normal resistances of the detectors, R_N, and the thermal conductivities, G. The first column of 32 detectors prepared for testing in CCam was composed of eight groups of four detectors with variable leg thicknesses connecting them to the bath. These bolometers were fabricated to allow us to measure the thermal conductivities, G (Figure 1), of the legs, so that we could choose the optimal leg width for the ACT detectors. In particular, we servo the temperature of the bath, T_{bath}, to a constant value below the TES critical temperature, T_c, and sweep the value of the bias applied to the detector and shunt resistor parallel circuit. We start the sweep in the voltage biased regime ($R_{TES} \gg R_{shunt}$) by briefly applying a ~ 2 mA bias to drive the TESs normal. The bias is gradually ramped down while acquiring TES $I-V$ curves (Figure 5) by measuring the change in TES current through the multiplexed SQUID readout electronics.

After proper normalization, the $I-V$ curve data is converted into the resistance versus power plane. In this plane we measure the normal resistance of the TESs as well as select an operating point on the superconducting transition that is some percentage of R_N. By acquiring $I-V$ curves at a variety of bath temperatures, we measure the change in Joule heating power, V_{bias}^2/R_{TES}, along the superconducting transition. Fitting these data allows us to solve for the thermal conductivities of the different leg designs and select the designs that we plan to use for each of the ACT bands. The optical measurements described below were made using bolometers with 5 μm wide legs, which have $G \approx 60$ pW/K.[14]

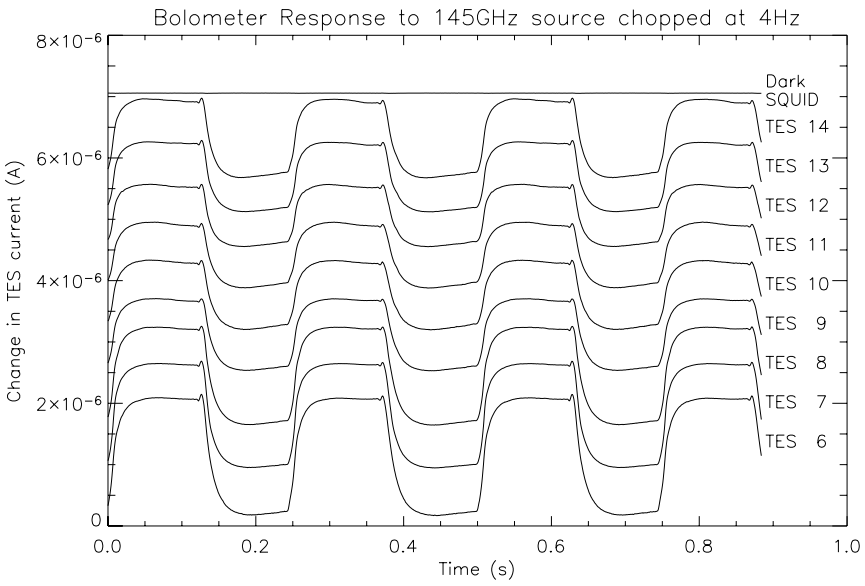

Figure 6. Bolometer responses to a 145 GHz source chopped at 4 Hz. The response of a Dark SQUID is also shown (top). Along the y-axis is relative current through the TESs, in which shifts have been added for plotting clarity. The decrease in peak-to-peak amplitude as a function of TES number is due to a gradient in the shunt resistances used to voltage bias the TESs. This gradient allowed us to probe bolometer responses at different points along the transition with a single measurement; also shown in the moon data (Figure 8). We will not, however, use shunt resistor chips with gradients this large in the MBAC arrays.

3.2. Optical Detector Tests

One of CCam's main goals was to confirm that we can measure two-millimeter radiation with one-millimeter TES bolometers without degradation of beam quality. The illumination of the detectors in CCam is controlled by a cold Lyot stop, three AR-coated silicon lenses,[8] and multiple filters, including low-pass filters and a bandpass filter developed by our collaborators at Cardiff University, UK. Prior to installing these filters and lenses into CCam, we measured their transmission on Fourier Transform Spectrometers (FTS). The combination of filters and lenses were found to have $\sim$ 80% efficiency at 145 GHz with 18 GHz FWHM bandpass. The bolometer response to a chopped 145 GHz source is shown in figure 6. More detailed efficiency measurements are ongoing.

Sky observations were made with CCam in Princeton, NJ by mounting the dewar onto a spare 1.5 m Gregorian telescope from the WMAP[22] experiment (Figure 7). We installed a 10% transmissive neutral density filter to prevent the high level of precipitable water vapor in New Jersey from saturating the detectors. Initial observations were made of the Moon to verify detector response, calibrate the pointing of the telescope and study the optical system sidelobes. Not surprisingly, scanning across the moon saturated many of the detectors, except those that were biased low on the transition, $R_{bias} \leq\sim R_N/4$ (Figure 8). Since the bolometer responsivity is non-linear and depends on a number of TES parameters that vary across the transition, point sources like bright planets are required to accurately measure small amplitude power absorption by the bolometers. To study this, a series of scanning measurements of Mars and Saturn were made, and we are currently in the process of analyzing the data from them. Among other things, these data will enable us to determine the total efficiency of the optical path including the absorption efficiency of the bolometers and the beam quality.

Detector measurements to complete our understanding of the detector model for MBAC and to test the ACT optics are also planned or underway. At Princeton there are dip probes for testing multiplexing chips, detector parameters, including noise characteristics and complex impedance of the bolometers,[14] and assembled arrays prior to installation into MBAC. The MBAC dewar is undergoing cryogenic testing at the University of Pennsylvania. In CCam, we are beginning to test folded bolometers with a new TES and absorber design. We

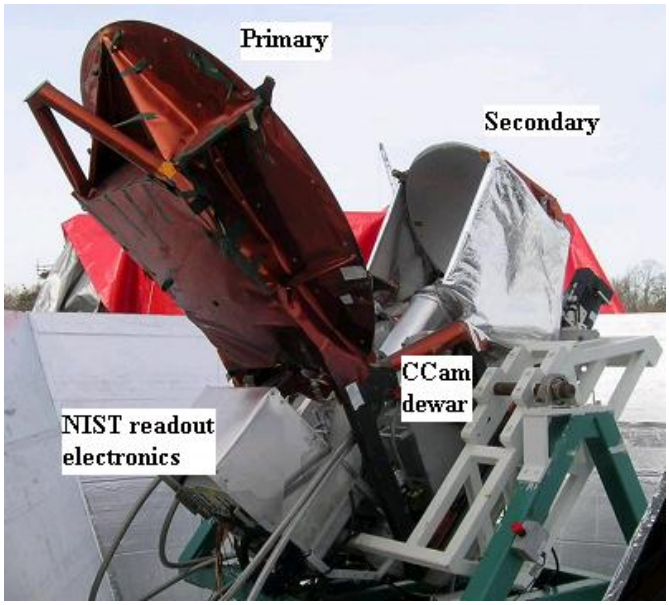

Figure 7. CCam dewar mounted onto the WMAP telescope[22] for sky observations in Princeton, NJ.

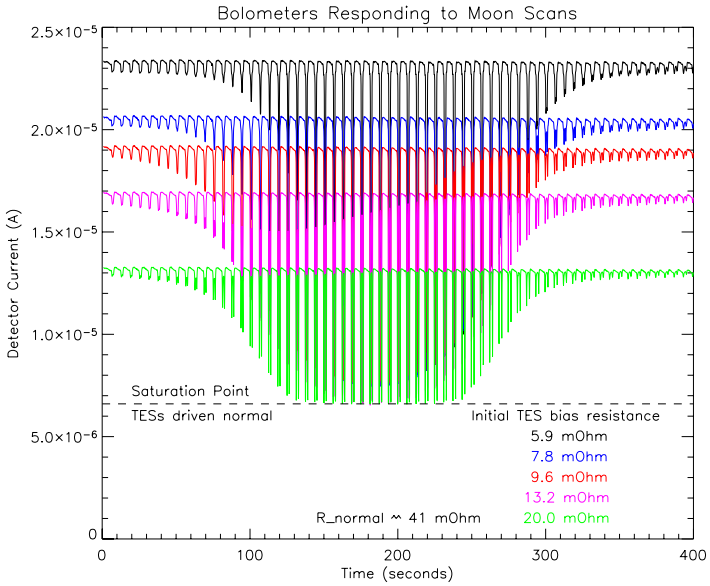

Figure 8. Bolometers responding to azimuthal scanning across the moon. The currents through five TESs that were biased to different points on their transitions are plotted. Since SQUIDs have arbitrary offsets in their readout, the absolute current (shown here) must be calibrated by analyzing an I-V curve acquired under similar loading conditions without the moon. As the photon loading from the moon increases, the TES resistances increase, causing a decrease in current through the TESs. The minimum current results from saturation of the bolometers when the TESs are driven to their normal resistance ($R_N = 41 \pm 3$ mΩ for this test device). The TESs are offset in azimuth from each other due to their position in the column, so that the top, black TES only observed the moon at the edge of the scan, and thus, its response profile is shifted in time with respect to the others because of the azimuthal motion of the moon.

are preparing to take both the MBAC cryostat and CCam to AMEC in Vancouver to use them for the initial acceptance testing of the ACT telescope in May-June, 2006.

4. CONCLUSIONS

Testing of many of the design principles for MBAC has been accomplished in CCam, and more detailed tests and analyses are underway. We have measured two-mm radiation with multiplexed one-mm TES PUD bolometers and detected astrophysical sources with them. Analyses are underway to confirm our understanding of the efficiencies of the bolometers and optical path as well as to test the predictions of the optical design. The initial construction of the ACT telescope in Vancouver is nearing completion; it is scheduled to be installed for use in Chile in the fourth quarter of 2006.

Acknowledgments

Thank you to all members of the ACT Collaboration for their contributions to this research, especially those at NIST, GSFC, UPenn, Cardiff, and U. Toronto for the multiplexing chips, detectors, helium refrigerator designs, filters, and cryogenic temperature measurement system used in CCam. Asad Aboobaker, Judy Lau, Eric Switzer, Adam Hincks, Toby Marriage, Ryan Fisher, Norm Jarosik, Joe Fowler, Suzanne Staggs, and Lyman Page contributed substantially to the CCam prototype instrument and the measurements described in this paper. The TES bolometers used in the tests described here were fabricated by J. Chervenak, D. J. Talley, J. A. Abrahams, and C. A. Allen at NASA GSFC's Detector Development Laboratory. We would also like to thank M. Halpern's group at UBC and J. Ruhl's group at Case Western for supporting our use of their FTSs. This work was supported by NSF award AST-0408698 for the ACT project, with additional support for M. Niemack from 2004 and 2005 SPIE Educational Scholarships in Optical Science and Engineering.

REFERENCES

1. A. Kosowsky, "The Atacama Cosmology Telescope," *New Astronomy Review* **47**, pp. 939–943, 2003.
2. J. Fowler for the ACT Collaboration, "The Atacama Cosmology Telescope project," *Proc. SPIE Millimeter and Submillimeter Detectors for Astronomy II* **5498**, pp. 1–10, 2004.
3. C. L. Bennett, M. Halpern, G. Hinshaw, N. Jarosik, A. Kogut, M. Limon, S. S. Meyer, L. Page, D. N. Spergel, G. S. Tucker, E. Wollack, E. L. Wright, C. Barnes, M. R. Greason, R. S. Hill, E. Komatsu, M. R. Nolta, N. Odegard, H. V. Peiris, L. Verde, and J. L. Weiland, "First year WMAP observations: Preliminary maps and basic results," *Astrophysical Jornal Supplement Series* **148**, pp. 1–27, 2003.
4. X. Wang, M. Tegmark, B. Jain, and M. Zaldarriaga, "The last stand before MAP: cosmological parameters from lensing, CMB and galaxy clustering," *Physical Review D* **68**, p. 123001, 2003.
5. D. Barbosa, J. G. Bartlett, and A. Blanchard, "Constraining Ω_0 with Sunyaev-Zeldovich observations," *Astrophysics & Space Science* **261**, pp. 277–280, 1998.
6. J. Ostriker and E. Vishniac, "Generation of microwave background fluctuations from nonlinear perturbations at the era of galaxy formation," *Astrophysical Journal* **306**, pp. L51–54, 1986.
7. D. Benford, J. Chervenak, K. Irwin, and H. Moseley, "Ultralow-background large-format bolometer arrays," *Proc. SPIE IR Space Telescopes and Instruments* **4850**, pp. 944–953, 2003.
8. J. Lau, J. Fowler, T. Marriage, L. Page, J. Leong, E. Wishnow, R. Henry, E. Wollack, M. Halpern, D. Marsden, and G. Marsden, "A millimeter-wave antireflection coating for cryogenic silicon lenses," *Applied Optics* , 2006 in press.
9. M. Niemack, S. Dicker, and J. Fowler for the ACT collaboration, "Optical design of the Atacama Cosmology Telescope and Millimeter Bolometer Array Camera," *Applied Optics* , 2006 in preparation.
10. A. T. Lee, P. L. Richards, S. W. Nam, B. Cabrera, and K. D. Irwin, "A superconducting bolometer with strong electrothermal feedback," *Appl. Phys. Lett.* **69**(12), pp. 1801–3, 1996.
11. K. Irwin and G. Hilton, *Transition-Edge Sensors, from Cryogenic Detectors*, Springer, 2005 preprint.
12. J. A. Chervenak, K. D. Irwin, E. N. Grossman, J. M. Martinis, C. D. Reintsema, and M. E. Huber, "Superconducting multiplexer for arrays of transition edge sensors," *Applied Physics Letters* **74**(26), pp. 4043–5, 1999.

13. C. D. Reintsema, J. Beyer, S. W. Nam, S. Deiker, G. C. Hilton, K. D. Irwin, J. M. Martinis, J. Ullom, L. R. Vale, and M. MacIntosh, "A prototype system for SQUID multiplexing of large-format transition-edge sensor arrays," *Review of Scientific Instruments* **74**, p. 4500, 2003.
14. T. Marriage, J. Chervenak, and R. Doriese, "Testing and assembly of the detectors for the Millimeter Bolometer Array Camera on ACT," *Nuclear Instruments and Methods in Physics Research A* **559**, pp. 551–553, 2006.
15. M. Griffin, J. Bock, and W. Gear, "Relative performance of filled and feedhorn-coupled focal-plane architectures," *Applied Optics* **41**(31), pp. 6543–6554, 2002.
16. M. Tinkham, *Introduction to Superconductivity*, McGraw-Hill, New York, NY, 1996.
17. M. Audley, W. Holland, T. Hodson, M. MacIntosh, I. Robson, K. Irwin, G. Hilton, W. Duncan, C. Reintsema, A. Walton, W. Parkes, P. Ade, I. Walker, M. Fich, J. Kycia, M. Halpern, D. Naylor, G. Mitchell, and P. Bastien, "An update on the SCUBA-2 project," *Proc. SPIE Millimeter and Submillimeter Detectors for Astronomy II* **5498**, pp. 63–77, 2004.
18. M. Niemack, "Multiplexing developments for the Atacama Cosmology Telescope," Master's thesis, Princeton University Physics Department, 2004.
19. P. A. de Korte, J. Beyer, S. Deiker, G. C. Hilton, K. D. Irwin, M. MacIntosh, S. W. Nam, C. D. Reintsema, L. R. Vale, and M. E. Huber, "Time-division superconducting quantum interference device multiplexer for transition-edge sensors," *Review of Scientific Instruments* **74**(8), pp. 3807–3815, 2003.
20. R. Doriese, "ACT detector preliminary design review documentation." ACT collaboration internal memo, 2004.
21. A. J. Mager, "Magnetic shields," *IEEE Trans. on Magnetics* **6**(1), pp. 67–75, 1970.
22. L. Page, C. Jackson, C. Barnes, C. Bennett, M. Halpern, G. Hinshaw, N. Jarosik, A. Kogut, M. Limon, S. Meyer, D. Spergel, G. Tucker, D. Wilkinson, E. Wollack, and E. Wright, "The optical design and characterization of the microwave anisotropy probe," *Astrophysical Journal* **585**, 2003.